Spectroscopy of ^{157}Yb and structure evolutions in odd-*A* Yb isotopes

C. Xu,[1] H. Hua,[1,*] X. Q. Li,[1,†] S. Q. Zhang,[1] J. Meng,[1] Z. H. Li,[1] F. R. Xu,[1] Y. Y. Cheng,[1] C. He,[1] J. J. Sun,[1] Y. Shi,[1] H. L. Liu,[1] Z. Y. Li,[2] L. H. Zhu,[3] X. G. Wu,[4] G. S. Li,[4] C. Y. He,[4] Y. Zheng,[4] S. G. Zhou,[5,6] S. Y. Wang,[7] Y. L. Ye,[1] D. X. Jiang,[1] T. Zheng,[1] J. L. Lou,[1] L. Y. Ma,[1] E. H. Wang,[1] L. L. Wang,[4] and B. Zhang[4]

[1]*School of Physics and State Key Laboratory of Nuclear Physics and Technology, Peking University, Beijing 100871, China*

[2]*College of Nuclear Science and Technology, Harbin Engineering University, Harbin 150001, China*

[3]*School of Physics and Nuclear Energy Engineering, Beihang University, Beijing 100191, China*

[4]*China Institute of Atomic Energy, Beijing 102413, China*

[5]*Institute of Theoretical Physics, Chinese Academy of Sciences, Beijing 100190, China*

[6]*Center of Theoretical Nuclear Physics, National Laboratory of Heavy Ion Accelerator, Lanzhou 730000, China*

[7]*Shandong Provincial Key Laboratory of Optical Astronomy and Solar-Terrestrial Environment, School of Space Science and Physics, Shandong University at Weihai, Weihai 264209, China*

(Received 11 October 2012; revised manuscript received 3 February 2013; published 26 March 2013)

The spectroscopy of ^{157}Yb has been studied via ^{144}Sm(^{16}O,3n)^{157}Yb fusion-evaporation reaction. The properties of bands associated with the $\nu i_{13/2}$ orbital and $\nu h_{9/2}$ orbital in ^{157}Yb are analyzed in comparison with the triaxial particle-rotor-model calculations. The characters of signature splitting for both positive-parity $\nu i_{13/2}$ and negative-parity $\nu h_{9/2}$ bands in ^{157}Yb and heavier odd-*A* Yb isotopes are discussed. The newly observed bands 1 and 2 in ^{157}Yb are suggested to be the signature partners of the $\nu h_{9/2}$ band. A systematic study of the band crossing frequencies associated with the $i_{13/2}$ neutron-pair and $h_{11/2}$ proton-pair alignments for the Yb isotopes, as well as the Er and Hf isotopes, are made.

DOI: 10.1103/PhysRevC.87.034325 PACS number(s): 21.10.Re, 23.20.Lv, 25.70.Gh, 27.70.+q

I. INTRODUCTION

Signature-splitting and band-crossing phenomena have been observed in many nuclei in the rare-earth region. Because the magnitude of signature splitting and the frequency at which band crossing occurs contain a wealth of nuclear structure information, such as the nuclear shapes, pairing correlations, and the changing behavior of configurations, they have long been of great interest in nuclear structure physics and attracted a lot of experimental and theoretical attention [1–14].

The present investigation is part of our program to study the nuclear properties of the light Yb isotopes. For the light Yb isotopes, it is well known that there is a shape transition from sphericity near the closed shell ($N = 82$), through γ-unstable, to stable prolate-deformed shapes ($N > 88$). Owing to the especial softness of nuclear potential-energy surfaces in the transitional Yb nuclei, such shape transitions also involve coexisting configurations of different shapes, which can be easily changed by rotation and alignment. In our previous paper [15], the structure evolutions induced by the increase in angular momentum, as well as by the change in neutron number, in the light even-*A* Yb isotopes have been discussed. In Ref. [16], the structural characters of odd-*A* ^{157}Yb nucleus provide evidence for shape coexistence of three distinct shapes: prolate, triaxial, and oblate. In this paper, we report the results of a continuing investigation of structure behaviors in the ^{157}Yb nucleus.

Because the transitional Yb nuclei have a susceptible shape, small change in deformation will affect the filling sequence of the single-particle orbitals and pairing correlations of the system. Thus, analyzing the characteristic signature splitting and seeing how the signature splitting evolves in the Yb isotope chain can bring valuable information regarding the underlying nuclear structures of the transitional Yb nuclei. In addition, in the light rare-earth region, the alignments of the $\nu i_{13/2}$, $\nu h_{9/2}$, and $\pi h_{11/2}$ pairs were suggested to play important roles in the band crossings. Their critical alignment frequencies were found to be close to each other and the relatively small shifts in alignment frequencies can replace one alignment with another. This character sometimes makes it difficult to unambiguously determine the cause of the alignments in these transitional nuclei. To get a comprehensive and clear understanding of the band crossing in this mass region, it is meaningful to make a systematic investigation of the band crossing. Here, with the new results of ^{157}Yb, the systematic characters of signature splitting and band crossing for the light odd-*A* Yb isotopes are studied.

II. EXPERIMENT RESULTS

The experiment was performed at the HI-13 tandem facility of the China Institute of Atomic Energy (CIAE). Detailed experimental description can be found in Ref. [16]. The partial level scheme with relative intensity of ^{157}Yb is shown in Fig. 1. The excitation energies, γ-ray energies, γ-ray transition intensities, DCO ratios, and spin-parity assignments for the ^{157}Yb nucleus are summarized in Table I. In general, stretched quadrupole transitions are adopted if DCO ratios are larger than 1.0, and stretched dipole transitions are assumed if DCO ratios are less than 0.8. The newly observed bands 1, 2, and 3 in ^{157}Yb have been reported in our previous paper [16]. In Ref. [16], the low-lying part of band 3 in ^{157}Yb was proposed

*hhua@pku.edu.cn
†lixq2002@pku.edu.cn

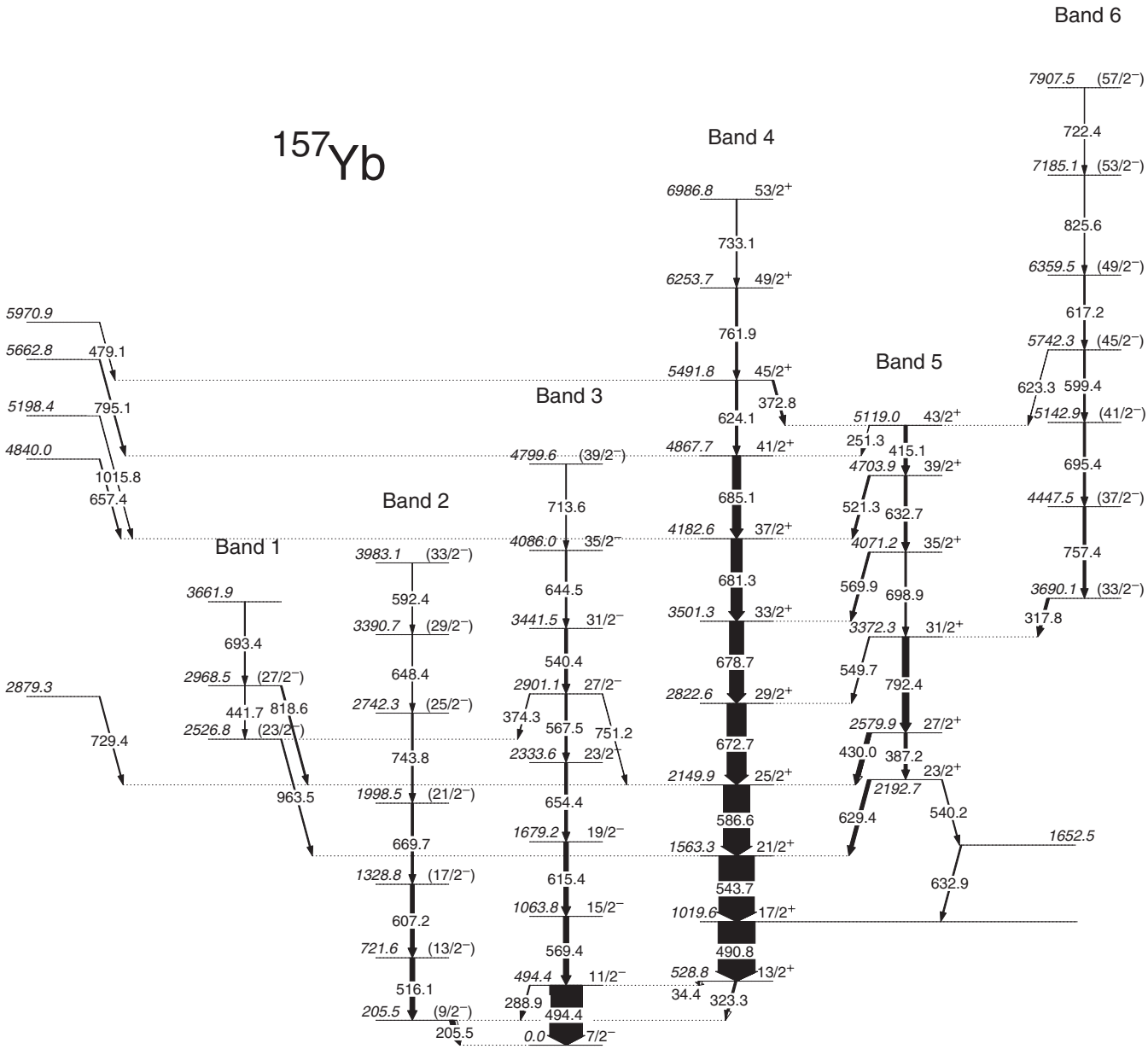

FIG. 1. Partial level scheme of ^{157}Yb. Energies are in keV.

to have a prolate deformation, while the low-lying part of band 4 was associated with a triaxial shape and bands 5 and 6 were suggested to have oblate deformations. The bands 3, 4, 5, and 6 have been discussed in terms of shape coexistence. At that time, no spins and parities were assigned to the three states in band 1. Here, the careful DCO analyses suggest the stretched dipole natures for the 963.5- and 818.6-keV transitions between band 1 and band 4, while the quadrupole assignment is made for the 374.3-keV transition between band 1 and band 3. Thus, the levels at 2526.8 and 2968.5 keV in band 1 are tentatively assigned spins and parities $23/2^-$ and $27/2^-$, respectively. The characters of the 963.5- and 818.6-keV interband transitions are very similar to those of the interband $E1$ transitions observed in the heavier odd-A Yb isotopes [1–3,17–19] and will be further discussed in Sec. IV.

III. STRUCTURES OF ROTATIONAL BANDS BASED ON THE $\nu i_{13/2}$ AND $\nu h_{9/2}$ CONFIGURATIONS

For the light Yb isotopes outside the $N = 82$ major shell, their excited states involve mainly neutrons occupying the $f_{7/2}$, $h_{9/2}$, and $i_{13/2}$ orbitals. According to the previous g-factor measurement [20], the bandhead $13/2^+$ of band 4 in ^{157}Yb was reported to have a quite pure $\nu i_{13/2}$ configuration, while the bandhead $9/2^-$ of band 2 was assumed to have the $\nu h_{9/2}$ configuration on the basis of good experimental level systematics of $N = 87$ even-Z isotones [16]. Here, to get a microscopic understanding of the band properties of ^{157}Yb, particle-rotor-model (PRM) calculations [21] have been performed to interpret the nature of these two bands. Detailed description of the PRM can be found in Refs. [21–24]. In the present calculations, the values of κ and μ in the Nilsson-type

TABLE I. γ-ray energies, excitation energies, relative γ-ray intensities, and DCO ratios in ^{157}Yb.

E_γ (keV)[a]	E_i (keV)	E_f (keV)	Int. (%)	DCO ratio	The γ-ray gate for DCO ratio (keV)	Assignment
205.5	205.5	0.0	13.9(2)	0.82(4)	516.1	$(9/2^-) \rightarrow 7/2^-$
251.3	5119.0	4867.7	0.8(1)			$43/2^+ \rightarrow 41/2^+$
288.9	494.4	205.5	2.3(2)	0.90(9)	490.8	$11/2^- \rightarrow (9/2^-)$
317.8	3690.1	3372.3	7.4(3)	0.59(3)	490.8	$(33/2^-) \rightarrow 31/2^+$
323.3	528.8	205.5	4.0(2)	0.84(9)	490.8	$13/2^+ \rightarrow (9/2^-)$
372.8	5491.8	5119.0	4.9(4)	0.96(6)	490.8	$45/2^+ \rightarrow 43/2^+$
374.3	2901.1	2526.8	2.0(2)	1.05(43)	644.5	$27/2^- \rightarrow (23/2^-)$
387.2	2579.9	2192.7	8.6(2)	1.00(6)	490.8	$27/2^+ \rightarrow 23/2^+$
415.1	5119.0	4703.9	9.0(2)	1.00(5)	490.8	$43/2^+ \rightarrow 39/2^+$
430.0	2579.9	2149.9	11.9(3)	0.98(4)	490.8	$27/2^+ \rightarrow 25/2^+$
441.7	2968.5	2526.8	0.9(2)			$(27/2^-) \rightarrow (23/2^-)$
479.1	5970.9	5491.8	1.2(2)			
490.8	1019.6	528.8	100	1.06(2)	494.4	$17/2^+ \rightarrow 13/2^+$
494.4	494.4	0.0	88.7(4)	1.06(2)	543.7	$11/2^- \rightarrow 7/2^-$
516.1	721.6	205.5	13.0(2)	1.09(5)	607.2	$(13/2^-) \rightarrow (9/2^-)$
521.3	4703.9	4182.6	5.5(1)	0.65(9)	490.8	$39/2^+ \rightarrow 37/2^+$
540.2	2192.7	1652.5	2.7(7)			
540.4	3441.5	2901.1	8.0(6)	0.97(7)	615.4	$31/2^- \rightarrow 27/2^-$
543.7	1563.3	1019.6	96.3(22)	1.04(1)	490.8	$21/2^+ \rightarrow 17/2^+$
549.7	3372.3	2822.6	3.0(1)	0.69(8)	543.7	$31/2^+ \rightarrow 29/2^+$
567.5	2901.1	2333.6	6.0(8)	0.95(7)	654.4	$27/2^- \rightarrow 23/2^-$
569.4	1063.8	494.4	14.4(16)	1.08(5)	654.4	$15/2^- \rightarrow 11/2^-$
569.9	4071.2	3501.3	5.6(6)	0.78(10)	490.8	$35/2^+ \rightarrow 33/2^+$
586.6	2149.9	1563.3	71.6(20)	1.02(2)	490.8	$25/2^+ \rightarrow 21/2^+$
592.4	3983.1	3390.7	0.6(1)			$(33/2^-) \rightarrow (29/2^-)$
599.4	5742.3	5142.9	4.8(3)	1.03(6)	757.4	$(45/2^-) \rightarrow (41/2^-)$
607.2	1328.8	721.6	10.5(4)	0.94(5)	516.1	$(17/2^-) \rightarrow (13/2^-)$
615.4	1679.2	1063.8	12.3(10)	1.03(5)	654.4	$19/2^- \rightarrow 15/2^-$
617.2	6359.5	5742.3	3.9(2)	0.96(9)	757.4	$(49/2^-) \rightarrow (45/2^-)$
623.3	5742.3	5119.0	0.9(1)			$(45/2^-) \rightarrow 43/2^+$
624.1	5491.8	4867.7	6.5(4)	0.96(7)	490.8	$45/2^+ \rightarrow 41/2^+$
629.4	2192.7	1563.3	9.7(2)	0.83(10)	490.8	$23/2^+ \rightarrow 21/2^+$
632.7	4703.9	4071.2	8.4(1)	0.98(6)	543.7	$39/2^+ \rightarrow 35/2^+$
632.9	1652.5	1019.6	3.5(1)			
644.5	4086.0	3441.5	4.2(2)	1.08(7)	654.4	$35/2^- \rightarrow 31/2^-$
648.4	3390.7	2742.3	1.9(2)	1.25(12)	607.2	$(29/2^-) \rightarrow (25/2^-)$
654.4	2333.6	1679.2	7.8(3)	1.03(7)	615.4	$23/2^- \rightarrow 19/2^-$
657.4	4840.0	4182.6	2.6(4)			
669.7	1998.5	1328.8	6.0(4)	1.11(6)	607.2	$(21/2^-) \rightarrow (17/2^-)$
672.7	2822.6	2149.9	51.8(9)	0.93(2)	490.8	$29/2^+ \rightarrow 25/2^+$
678.7	3501.3	2822.6	38.5(8)	1.02(9)	490.8	$33/2^+ \rightarrow 29/2^+$
681.3	4182.6	3501.3	30.4(7)	1.10(11)	543.7	$37/2^+ \rightarrow 33/2^+$
685.1	4867.7	4182.6	22.6(4)	1.04(11)	543.7	$41/2^+ \rightarrow 37/2^+$
693.4	3661.9	2968.5	2.6(4)			
695.4	5142.9	4447.5	6.1(5)	1.06(6)	757.4	$(41/2^-) \rightarrow (37/2^-)$
698.9	4071.2	3372.3	4.5(5)	1.02(7)	543.7	$35/2^+ \rightarrow 31/2^+$
713.6	4799.6	4086.0	2.0(8)			$(39/2^-) \rightarrow 35/2^-$
722.4	7907.5	7185.1	1.2(1)			$(57/2^-) \rightarrow (53/2^-)$
729.4	2879.3	2149.9	2.6(1)			
733.1	6986.8	6253.7	3.1(1)	1.07(12)	672.7	$53/2^+ \rightarrow 49/2^+$
743.8	2742.3	1998.5	4.7(3)	0.95(7)	607.2	$(25/2^-) \rightarrow (21/2^-)$
751.2	2901.1	2149.9	1.3(1)			$27/2^- \rightarrow 25/2^+$
757.4	4447.5	3690.1	7.4(2)	1.04(7)	543.7	$(37/2^-) \rightarrow (33/2^-)$
761.9	6253.7	5491.8	5.8(2)	0.99(9)	672.7	$49/2^+ \rightarrow 45/2^+$
792.4	3372.3	2579.9	18.0(3)	0.97(5)	543.7	$31/2^+ \rightarrow 27/2^+$
795.1	5662.8	4867.7	3.2(1)			

TABLE I. (*Continued*).

E_γ (keV)[a]	E_i (keV)	E_f (keV)	Int. (%)	DCO ratio	The γ-ray gate for DCO ratio (keV)	Assignment
818.6	2968.5	2149.9	4.3(1)	0.61(29)	543.7	$(27/2^-) \rightarrow 25/2^+$
825.6	7185.1	6359.5	1.8(1)			$(53/2^-) \rightarrow (49/2^-)$
963.5	2526.8	1563.3	3.2(1)	0.61(37)	543.7	$(23/2^-) \rightarrow 21/2^+$
1015.8	5198.4	4182.6	1.4(1)			

[a]Uncertainties between 0.1 and 0.5 keV.

Hamiltonian are taken from Ref. [25]; i.e., $\kappa = 0.062$ and $\mu = 0.43$ for the main oscillator quantum number $N = 5$, and $\kappa = 0.062$ and $\mu = 0.34$ for $N = 6$. The quadrupole deformation parameter ε_2 and the triaxiality parameter γ are adopted from the total Routhian surface (TRS) calculations [26,27]; i.e., for the positive-parity $\nu i_{13/2}$ band, $\varepsilon_2 = 0.161$ and $\gamma = 21^\circ$, while for the negative-parity $\nu h_{9/2}$ band, $\varepsilon_2 = 0.152$ and $\gamma = 3^\circ$. The hexadecapole deformation is neglected in the present PRM investigation. For all the present calculations, an off-diagonal Coriolis attenuation parameter $\xi = 0.7$ [23], as well as a variable moment of inertia, $\mathcal{J}_0(I) = \mathcal{J}_0\sqrt{1 + bI(I+1)}$ [28], is used. The pairing factors are taken according to Ref. [29].

For the axially deformed case, the orbitals are usually denoted by the Nilsson quantum number $\Omega^\pi[Nn_3\Lambda]$. For the triaxially deformed case, because Ω is not a good quantum number, the number ν is used to denote the single-particle state according to the sequence of the energy. For convenience, the Nilsson quantum number is also used to denote approximately the single-particle state in the triaxially deformed case. In Tables II and III, nine positive-parity orbitals near the neutron Fermi level at $(\varepsilon_2, \gamma) = (0.161, 21^\circ)$ and nine negative-parity orbitals at $(\varepsilon_2, \gamma) = (0.152, 3^\circ)$ adopted in the present triaxial PRM calculations are listed. These orbitals are used to couple with the core in the calculations for the positive-parity and negative-parity bands of ^{157}Yb, respectively. Their approximate Nilsson quantum numbers, single-particle energies, and main components expanded in the basis $|Nlj\Omega\rangle$ are also shown. The neutron Fermi energy λ_n is 50.46 MeV at $(0.161, 21^\circ)$ and 50.47 MeV at $(0.152, 3^\circ)$, respectively. From Tables II and III, one can see that the main component for the positive-parity orbitals near the Fermi level is $\nu i_{13/2}\ 1/2^+[660]$, while for the negative-parity orbitals there is a strong mixture of $h_{9/2}$ and $f_{7/2}$ subshells.

Using the triaxial PRM, the energy spectra of the positive-parity $\nu i_{13/2}$ band (band 4) and the negative-parity $\nu h_{9/2}$ band (band 2) in ^{157}Yb are calculated and illustrated in Figs. 2(a) and 2(b), respectively. As seen from Fig. 2, the triaxial PRM calculations reproduce reasonably the energy spectra of the $\nu i_{13/2}$ band and the $\nu h_{9/2}$ band of ^{157}Yb. The main components of the wave functions for the state sequence at low-spin region $I = 13/2, 17/2, 21/2, 25/2, 29/2, 33/2, 37/2\hbar$ in the $\nu i_{13/2}$ band and $I = 9/2, 13/2, 17/2, 21/2, 25/2, 29/2, 33/2\hbar$ in the $\nu h_{9/2}$ band are listed in Table IV. For the $\nu i_{13/2}$ band, the orbital $|5\rangle$ (corresponding to $1/2^+[660]$) is the dominant component at the bandhead ($\sum_K |C_5^{IK}|^2 \sim 89.1\%$), which agrees with the previous configuration assignment [20] very well. As the nucleus rotates faster, the contribution from the orbital $|5\rangle$ ($1/2^+[660]$) decreases gradually. For the $\nu h_{9/2}$ band, the orbital $|5\rangle$ ($3/2^-[521]$) is the dominant component of the 9/2 sequence. Although the orbital $|3\rangle$ ($1/2^-[530]$) is closer to the Fermi surface than the orbital $|5\rangle$ and also has the $\nu h_{9/2}$ configuration as the dominant component, the PRM calculations indicate that the decoupling effect of orbital $|3\rangle$ is very strong owing to its main quantum number $K = 1/2$ and the small triaxial deformation parameter $\gamma = 3^\circ$. This strong decoupling effect will result in that the eigenstates of PRM with orbital $|3\rangle$ as the main component are much higher in energy

TABLE II. The neutron positive-parity single-particle levels at $\varepsilon_2 = 0.161$, $\gamma = 21^\circ$ adopted for the present triaxial PRM calculations. The approximate Nilsson quantum numbers, single-particle energies, and main components expanded in the basis $|Nlj\Omega\rangle$ are shown. The neutron Fermi energy λ_n is ~50.46 MeV.

$\|\nu\rangle$	$\Omega^\pi[Nn_z\Lambda]$	ε_ν (MeV)	Main components in terms of $\|Nlj\Omega\rangle$
$\|1\rangle$	$1/2^+[411]$	46.17	$0.584\|4d_{3/2}\,\frac{1}{2}\rangle - 0.470\|4s_{1/2}\,\frac{1}{2}\rangle - 0.363\|4g_{7/2}\,\frac{1}{2}\rangle$
$\|2\rangle$	$7/2^+[404]$	46.24	$0.927\|4g_{7/2}\,\frac{7}{2}\rangle - 0.288\|4d_{3/2}\,\frac{3}{2}\rangle - 0.164\|4d_{3/2}\,\frac{1}{2}\rangle$
$\|3\rangle$	$1/2^+[400]$	47.49	$0.558\|4d_{3/2}\,\frac{3}{2}\rangle + 0.549\|4s_{1/2}\,\frac{1}{2}\rangle + 0.434\|4d_{3/2}\,\frac{1}{2}\rangle$
$\|4\rangle$	$3/2^+[402]$	48.66	$0.722\|4d_{3/2}\,\frac{3}{2}\rangle - 0.474\|4s_{1/2}\,\frac{1}{2}\rangle - 0.352\|4d_{3/2}\,\frac{1}{2}\rangle$
$\|5\rangle$	$1/2^+[660]$	51.49	$0.762\|6i_{13/2}\,\frac{1}{2}\rangle + 0.523\|6i_{13/2}\,\frac{3}{2}\rangle + 0.268\|6i_{13/2}\,\frac{5}{2}\rangle$
$\|6\rangle$	$3/2^+[651]$	52.23	$0.738\|6i_{13/2}\,\frac{3}{2}\rangle - 0.420\|6i_{13/2}\,\frac{5}{2}\rangle - 0.380\|6i_{13/2}\,\frac{1}{2}\rangle$
$\|7\rangle$	$5/2^+[642]$	52.73	$0.817\|6i_{13/2}\,\frac{5}{2}\rangle - 0.407\|6i_{13/2}\,\frac{1}{2}\rangle - 0.206\|6g_{9/2}\,\frac{1}{2}\rangle$
$\|8\rangle$	$7/2^+[633]$	53.31	$0.932\|6i_{13/2}\,\frac{7}{2}\rangle - 0.243\|6i_{13/2}\,\frac{3}{2}\rangle - 0.166\|6g_{9/2}\,\frac{3}{2}\rangle$
$\|9\rangle$	$9/2^+[624]$	54.10	$0.969\|6i_{13/2}\,\frac{9}{2}\rangle - 0.150\|4g_{9/2}\,\frac{5}{2}\rangle - 0.148\|6i_{13/2}\,\frac{5}{2}\rangle$

TABLE III. The neutron negative-parity single-particle levels at $\varepsilon_2 = 0.152$, $\gamma = 3^\circ$ adopted for the present triaxial PRM calculations. The approximate Nilsson quantum numbers, single-particle energies, and main components expanded in the basis $|Nlj\Omega\rangle$ are shown. The neutron Fermi energy λ_n is ∼50.47 MeV.

$\|\nu\rangle$	$\Omega^\pi[Nn_z\Lambda]$	ε_ν (MeV)	Main components in terms of $\|Nlj\Omega\rangle$
$\|1\rangle$	$11/2^-[505]$	48.79	$0.9998\|5h_{11/2}\,\frac{11}{2}\rangle - 0.018\|5f_{7/2}\,\frac{7}{2}\rangle - 0.006\|5h_{11/2}\,\frac{7}{2}\rangle$
$\|2\rangle$	$1/2^-[541]$	49.72	$0.758\|5f_{7/2}\,\frac{1}{2}\rangle + 0.423\|5p_{3/2}\,\frac{1}{2}\rangle - 0.310\|5h_{9/2}\,\frac{1}{2}\rangle$
$\|3\rangle$	$1/2^-[530]$	50.34	$0.779\|5h_{9/2}\,\frac{1}{2}\rangle + 0.322\|5f_{7/2}\,\frac{1}{2}\rangle + 0.319\|5f_{5/2}\,\frac{1}{2}\rangle$
$\|4\rangle$	$3/2^-[532]$	50.46	$0.656\|5f_{7/2}\,\frac{3}{2}\rangle + 0.507\|5h_{9/2}\,\frac{3}{2}\rangle - 0.334\|5h_{9/2}\,\frac{1}{2}\rangle$
$\|5\rangle$	$3/2^-[521]$	51.12	$0.769\|5h_{9/2}\,\frac{3}{2}\rangle - 0.592\|5f_{7/2}\,\frac{3}{2}\rangle + 0.148\|5f_{5/2}\,\frac{3}{2}\rangle$
$\|6\rangle$	$5/2^-[523]$	51.47	$0.771\|5h_{9/2}\,\frac{5}{2}\rangle - 0.583\|5f_{7/2}\,\frac{5}{2}\rangle + 0.197\|5f_{5/2}\,\frac{5}{2}\rangle$
$\|7\rangle$	$5/2^-[512]$	52.18	$0.783\|5f_{7/2}\,\frac{5}{2}\rangle + 0.612\|5h_{9/2}\,\frac{5}{2}\rangle - 0.106\|5h_{11/2}\,\frac{5}{2}\rangle$
$\|8\rangle$	$7/2^-[514]$	52.70	$0.916\|5h_{9/2}\,\frac{7}{2}\rangle + 0.387\|5f_{7/2}\,\frac{7}{2}\rangle - 0.101\|5h_{11/2}\,\frac{7}{2}\rangle$
$\|9\rangle$	$1/2^-[521]$	52.97	$0.535\|5f_{5/2}\,\frac{1}{2}\rangle + 0.498\|5p_{1/2}\,\frac{1}{2}\rangle - 0.454\|5p_{3/2}\,\frac{1}{2}\rangle$

than those with orbital $|5\rangle$ as the main component. Thus, the dominant component of the 9/2 sequence comes from orbital $|5\rangle$. The present triaxial PRM calculations further support the previous assignment [16] for the 9/2 sequence (band 2). As the nucleus rotates faster, the dominant component from orbital $|5\rangle$ decreases gradually, while the contribution from orbital $|3\rangle$ increases gradually.

IV. SIGNATURE SPLITTING

For the positive-parity $\nu i_{13/2}$ bands in light Yb isotopes, an interesting phenomenon is that the unfavored signature partner of the $\nu i_{13/2}$ band is not observed in ^{157}Yb ($N = 87$), while both the signature partners of the $\nu i_{13/2}$ bands have been found in the heavier odd-A Yb ($N \geqslant 89$) isotopes [1,3,18,19]. Here, the experimental values of signature splitting for the $\nu i_{13/2}$ bands at $\hbar\omega = 0.2$ MeV, which is below the first band crossing, as a function of neutron number for the light Yb isotopes are extracted and shown in Fig. 3. For a rotational band, the experimental signature splitting $\Delta e'$ is defined as the difference in energies at a given rotational frequency for the pair of signature partners: $\Delta e' = E^\omega_u - E^\omega_f$, where E^ω is the Routhian energy of the rotational band and is defined as $E^\omega = E(I) - \hbar\omega I_x$, where $E(I)$ is the energy of the level with spin I, $\hbar\omega = \frac{E(I+1)-E(I-1)}{I_x(I+1)-I_x(I-1)}$, $I_x = \sqrt{I(I+1) - K^2}$, and K represents the projection of angular momentum on the nuclear symmetry axis.

As shown in Fig. 3, the two signatures of the $\nu i_{13/2}$ bands in these odd-A Yb isotopes show considerable splitting at low rotational frequency and the magnitude of the signature splitting decreases while the neutron number increases. For

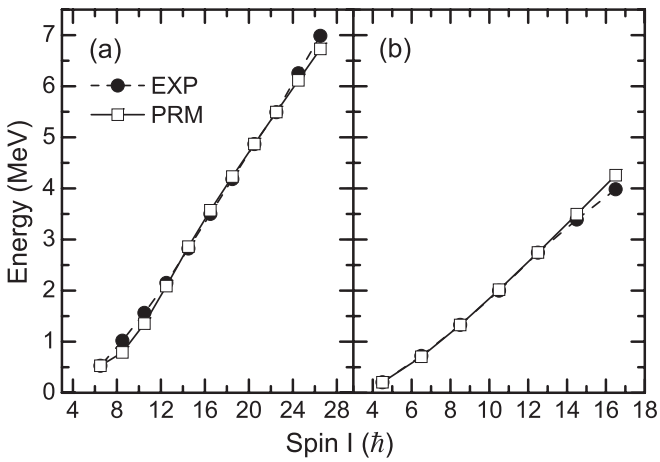

FIG. 2. The energy spectra $E(I)$ for (a) the positive-parity $\nu i_{13/2}$ band and (b) the negative-parity $\nu h_{9/2}$ band in ^{157}Yb based on the PRM calculations (open squares) in comparison with the experimental data (solid circles). A variable moment of inertia is applied in the PRM calculations with $\mathcal{J}_0 = 11.2$ MeV$^{-1}\hbar^2$ and $b = 0.013$ for the $\nu i_{13/2}$ band; $\mathcal{J}_0 = 10.6$ MeV$^{-1}\hbar^2$ and $b = 0.013$ for the $\nu h_{9/2}$ band.

TABLE IV. The main components expanded in the strong coupling basis $|IMK\nu\rangle$ (denoted as $|K\nu\rangle$ for short) for selected states in the positive-parity $\nu i_{13/2}$ band and negative-parity $\nu h_{9/2}$ band. The parameters in the calculations are the same as that in Fig. 2.

I^π	Main components in terms of $\|K\nu\rangle$
$\frac{13}{2}^+$	$0.754\|\frac{1}{2}\,5\rangle + 0.513\|\frac{3}{2}\,5\rangle + 0.244\|\frac{5}{2}\,5\rangle + 0.224\|\frac{3}{2}\,6\rangle$
$\frac{17}{2}^+$	$0.760\|\frac{1}{2}\,5\rangle + 0.513\|\frac{3}{2}\,5\rangle + 0.235\|\frac{5}{2}\,5\rangle + 0.225\|\frac{3}{2}\,6\rangle$
$\frac{21}{2}^+$	$0.777\|\frac{1}{2}\,5\rangle + 0.497\|\frac{3}{2}\,5\rangle + 0.243\|\frac{3}{2}\,6\rangle + 0.191\|\frac{5}{2}\,5\rangle$
$\frac{25}{2}^+$	$0.795\|\frac{1}{2}\,5\rangle + 0.445\|\frac{3}{2}\,5\rangle + 0.288\|\frac{3}{2}\,6\rangle - 0.157\|\frac{1}{2}\,6\rangle$
$\frac{29}{2}^+$	$0.767\|\frac{1}{2}\,5\rangle + 0.356\|\frac{3}{2}\,6\rangle + 0.321\|\frac{3}{2}\,5\rangle - 0.215\|\frac{1}{2}\,6\rangle$
$\frac{33}{2}^+$	$0.670\|\frac{1}{2}\,5\rangle + 0.404\|\frac{3}{2}\,6\rangle - 0.264\|\frac{1}{2}\,6\rangle - 0.248\|\frac{5}{2}\,5\rangle$
$\frac{37}{2}^+$	$0.575\|\frac{1}{2}\,5\rangle + 0.422\|\frac{3}{2}\,6\rangle - 0.317\|\frac{5}{2}\,5\rangle - 0.292\|\frac{1}{2}\,6\rangle$
$\frac{9}{2}^-$	$0.732\|\frac{3}{2}\,5\rangle - 0.527\|\frac{5}{2}\,6\rangle - 0.337\|\frac{5}{2}\,7\rangle - 0.227\|\frac{7}{2}\,8\rangle$
$\frac{13}{2}^-$	$0.708\|\frac{3}{2}\,5\rangle - 0.501\|\frac{5}{2}\,6\rangle - 0.368\|\frac{5}{2}\,7\rangle - 0.254\|\frac{7}{2}\,8\rangle$
$\frac{17}{2}^-$	$0.694\|\frac{3}{2}\,5\rangle - 0.479\|\frac{5}{2}\,6\rangle - 0.369\|\frac{5}{2}\,7\rangle - 0.251\|\frac{7}{2}\,8\rangle$
$\frac{21}{2}^-$	$0.680\|\frac{3}{2}\,5\rangle - 0.458\|\frac{5}{2}\,6\rangle - 0.357\|\frac{5}{2}\,7\rangle - 0.306\|\frac{1}{2}\,3\rangle$
$\frac{25}{2}^-$	$0.665\|\frac{3}{2}\,5\rangle - 0.436\|\frac{5}{2}\,6\rangle - 0.360\|\frac{1}{2}\,3\rangle - 0.340\|\frac{5}{2}\,7\rangle$
$\frac{29}{2}^-$	$0.648\|\frac{3}{2}\,5\rangle - 0.416\|\frac{5}{2}\,6\rangle - 0.408\|\frac{1}{2}\,3\rangle - 0.321\|\frac{5}{2}\,7\rangle$
$\frac{33}{2}^-$	$0.630\|\frac{3}{2}\,5\rangle - 0.449\|\frac{1}{2}\,3\rangle - 0.396\|\frac{5}{2}\,6\rangle - 0.303\|\frac{5}{2}\,7\rangle$

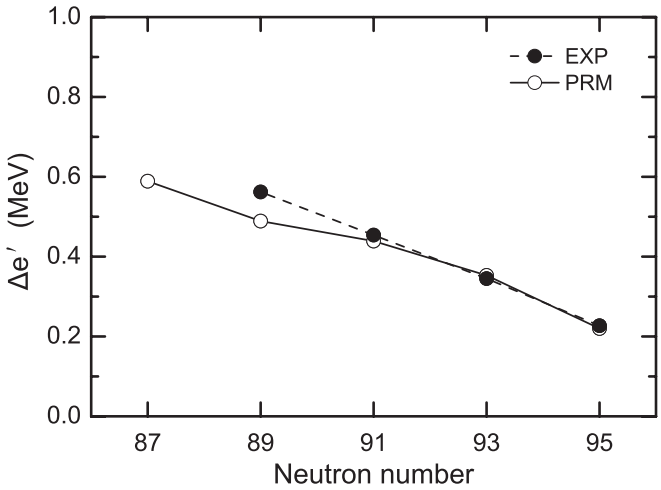

FIG. 3. Experimental (solid circles) and calculated (open circles) signature splitting ($\Delta e'$) for the positive-parity $\nu i_{13/2}$ bands at $\hbar\omega = 0.2$ MeV in the odd-A Yb isotopes. The data for the heavier Yb isotopes come from Ref. [18] (^{159}Yb), Ref. [30] (^{161}Yb), Ref. [3] (^{163}Yb), and Ref. [30] (^{165}Yb).

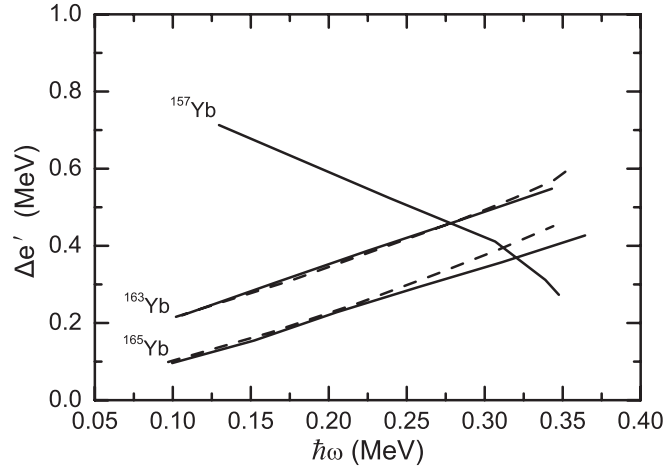

FIG. 4. Frequency dependence of the experimental (dashed lines) and theoretical (solid lines) signature splitting $\Delta e'$ for the positive-parity $\nu i_{13/2}$ bands of the ^{157,163,165}Yb isotopes.

the bands built on the high-j $\nu i_{13/2}$ Nilsson orbitals, it is known that the magnitude of signature splitting reflects an admixture of the $\Omega = 1/2$ orbital of $i_{13/2}$ shell in the wave function owing to the Coriolis interaction. According to the previous g-factor measurement [20] and the present PRM calculations, for the positive-parity orbitals, the neutron Fermi energy for ^{157}Yb nucleus is near the $\Omega = 1/2$ substate of the $\nu i_{13/2}$ shell and the dominant components of the low-spin states of $\nu i_{13/2}$ band in ^{157}Yb come from orbital $|5\rangle$ (corresponding to $1/2^+[660]$). Thus, the magnitude of signature splitting of $\nu i_{13/2}$ band in ^{157}Yb should be relatively large compared to the neighboring heavier Yb isotopes. The systematic features of signature splitting in $\nu i_{13/2}$ bands of light Yb isotopes can be explained by the shift of the Fermi surface away from the $1/2^+[660]$ Nilsson orbital with increasing neutron number.

In Fig. 3, the calculated signature splitting $\Delta e'$ using the PRM for the $\nu i_{13/2}$ bands of the Yb isotopes are also plotted and compared with the experimental data. The overall agreement between the experimental data and theoretical results is good. However, as shown in Fig. 3, except the ^{163}Yb and ^{165}Yb nuclei, the magnitude of the signature splitting for the $\nu i_{13/2}$ bands in the lighter transitional Yb isotopes is systematically underpredicted and the discrepancies between the calculated and experimental $\Delta e'$ increase with decreasing neutron number. Because the PRM assumes the nucleus has a rigid deformation, while in fact a γ-soft shape is predicted and the shape softness increases with decreasing neutron number for the lighter Yb isotopes, the small difference may be attributable to the influence of shape softness. According to the trend of the experimental signature splitting along with the neutron number and the theoretical calculations, the unfavored signature sequence of the $\nu i_{13/2}$ band in ^{157}Yb will have an excitation energy above the favored signature sequence as big as 600–800 keV at $\hbar\omega = 0.2$ MeV. Such a large signature splitting may explain why the corresponding unfavored signature partner sequence of the $\nu i_{13/2}$ band is not observed in the present study of ^{157}Yb nucleus.

In addition, as shown in Fig. 4, theoretical $\Delta e'$ for the positive-parity $\nu i_{13/2}$ band of ^{157}Yb is predicted to decrease with increasing rotation frequency, while both the experimental and the theoretical $\Delta e'$ for the heavier Yb isotopes such as ^{163}Yb and ^{165}Yb are found to increase with increasing rotation frequency. Shastry *et al.* [6] have ascribed this feature observed in the heavier Yb isotopes to the depression of the $\alpha = 1/2$ Routhian of the $\Omega = 1/2$ $i_{13/2}$ neutron orbital in energy with increasing the rotational frequency, which causes the component of $\Omega = 1/2$ $i_{13/2}$ neutron orbital to mix into the lowest $\alpha = 1/2$ positive-parity state and consequently produces the observed increase in signature splitting at large $\hbar\omega$. According to the present PRM calculations, as the nucleus rotates faster, the components of wave functions from the orbital $1/2^+[660]$ increase for the $\nu i_{13/2}$ bands of ^{163}Yb and ^{165}Yb nuclei, while the components in the ^{157}Yb nucleus will decrease gradually, as shown in Table IV. The trends of the wave functions of the $\nu i_{13/2}$ bands in ^{163}Yb and ^{165}Yb are consistent with the explanation by Shastry *et al.* [6]. At higher rotational frequency above the band crossing, the PRM calculations cannot well reproduce the observed signature splitting in the positve-parity $\nu i_{13/2}$ bands of ^{163}Yb and ^{165}Yb, because the self-consistent explanation of signature splitting above the band crossing is beyond the physical picture of one quasineutron coupled with a triaxially deformed core in the PRM.

Compared to the relative pure intruder $\nu i_{13/2}$ configuration, the characters of signature splitting in bands built on the nonintruder $\nu h_{9/2}$ orbitals in the Yb isotopes are complicated because of the strong mixing of the $\nu h_{9/2}$ configuration with other configurations, especially the component of the $\nu f_{7/2}$ orbital. Although both the signature partners of the $\nu h_{9/2}$ bands have been found in the heavier odd-A Yb ($N \geqslant 89$) isotopes, the low-lying parts of the unfavored $\nu h_{9/2}$ bands are all incomplete in these isotopes and several low-spin states of the unfavored structures are not experimentally observed. A common feature of these unfavored signature partners of the $\nu h_{9/2}$ bands in the odd-A Yb isotopes [1–3,17–19], as well as

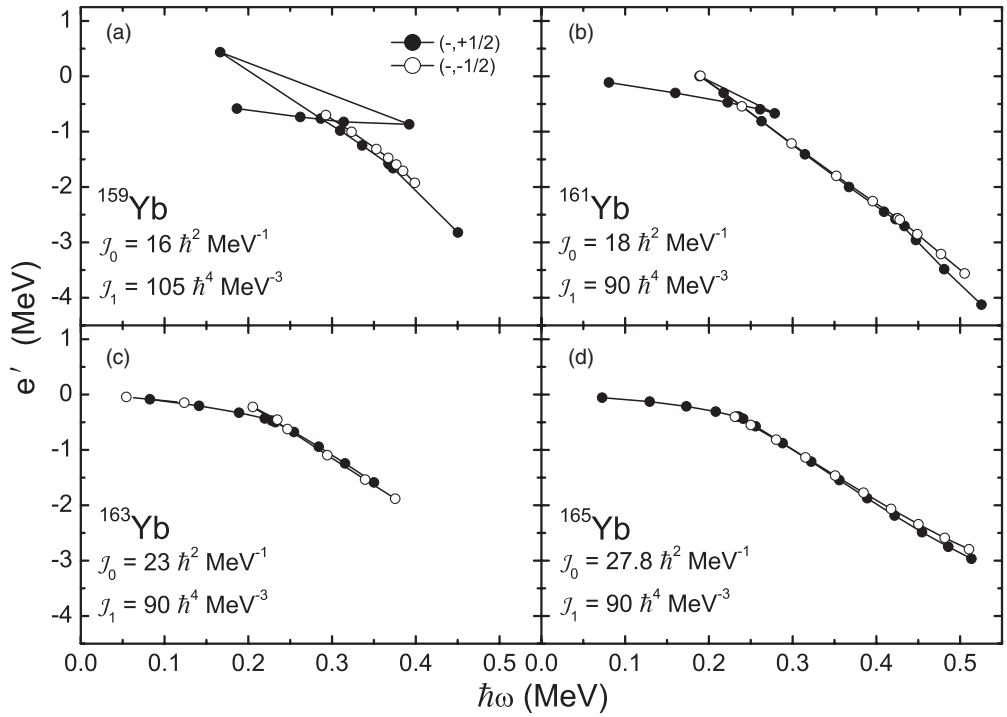

FIG. 5. Experimental Routhians e' extracted for the negative-parity $\nu h_{9/2}$ bands in (a)^{159}Yb, (b)^{161}Yb, (c)^{163}Yb, and (d)^{165}Yb isotopes.

the neighboring odd-A Er isotopes [31–33], is the observed $E1$ transitions between the $\nu h_{9/2}$ band and the $\nu i_{13/2}$ band. Compared to the expectation for single-particle transitions, these $E1$ transitions are found to be strongly enhanced. Hamamoto *et al.* [34,35] have systematically analyzed the $E1$ transitions in the odd-A rare-earth nuclei and found that the calculated $B(E1)$ values using the quadrupole deformation and the original $E1$ transition operator are too small to be detected in competition with rotational $E2$ transitions. According to their analyses, both the strength and the pattern of the $E1$ transitions can be successfully interpreted in terms of the coupling to the octupole vibrational degrees of freedom. Since the octupole bands have already been found in many even-even Yb isotopes such as ^{158}Yb [36], ^{160}Yb [1,37], ^{162}Yb [38], ^{164}Yb [5], and ^{166}Yb [5], the observed $E1$ transitions between bands 1 and 4 in ^{157}Yb indicate that the octupole vibration may also play an important role in the structure of ^{157}Yb. In addition, these observed $E1$ transitions in ^{157}Yb are very similar to the enhanced $E1$ transitions in the heavier Yb isotopes which connect the $(\pi, \alpha) = (-, -1/2)$ $\nu h_{9/2}$ band and the $(+, +1/2)$ $\nu i_{13/2}$ band [1–3,17–19]. This striking similarity indicates that bands 1 and 2 in ^{157}Yb may form the signature partners of the $h_{9/2}$ band. Owing to the enhanced interband $E1$ transitions dominating the intraband $E2$ transitions in the unfavored negative-parity $\nu h_{9/2}$ band in ^{157}Yb, the low-spin part of the unfavored signature partner of $\nu h_{9/2}$ band cannot be significantly populated. Consequently, the weak intraband $E2$ transition cascade in the low-spin region is difficult to be experimentally observed.

Because the low-spin parts of unfavored signature partners of $\nu h_{9/2}$ bands are not fully established in the light Yb isotopes, the experimental values of signature splitting for the $\nu h_{9/2}$ bands at low $\hbar\omega$ cannot been extracted. As shown in Fig. 5, a small positive signature splitting is observed at large values of $\hbar\omega$ for all the light odd-A Yb isotopes except the ^{163}Yb nucleus, where a small negative splitting is observed at large $\hbar\omega$, but a small positive splitting is observed at low $\hbar\omega$. Although the character of the $1/2^-[530]$ Nilsson orbit of the $h_{9/2}$ shell, which is the nearest $\Omega = 1/2$ orbit to the Fermi surface for the $\nu h_{9/2}$ bands in the light Yb isotopes, can account for the small experimental values of signature splitting in the light Yb isotopes, the unique feature of signature splitting observed in ^{163}Yb cannot be successfully explained by the cranked-shell-model (CSM) calculations [39], which predict a positive signature splitting for all the light Yb isotopes. In Ref. [3], Kownacki *et al.* have suggested this change in the sign of the signature splitting between low- and high-spin portions of the $\nu h_{9/2}$ band in ^{163}Yb may be caused by a relatively small change in quadrupole deformation for these configurations before and after the alignment of the pair of $i_{13/2}$ neutrons. According to our TRS calculations, the quadrupole deformation ε_2 of ^{163}Yb will change from 0.226 to 0.223 before and after a pair of $i_{13/2}$ neutron alignment, while the hexadecapole deformation ε_4 changes from -0.006 to 0.001 and the γ value remains constant during the same alignment process. The effect of hexadecapole deformation on the signature splitting has been discussed by Nyberg *et al.* [40]. They found that the change in the absolute value of hexadecapole deformation will alter the magnitude of signature splitting a lot. Thus, for ^{163}Yb nucleus, both the changes of quadrupole and hexadecapole deformations may affect the change in the sign of the signature splitting together. To get better understanding of the underlying

mechanism of the change in the sign, more theoretical and systematic studies are needed.

V. BAND CROSSING

The new results of ^{157}Yb together with the already known information on the neighboring Yb isotopes allow a systematic comparison of the band crossings occurring in the Yb isotopes. Here, the kinematic moments of inertia as a function of rotational frequency for the positive-parity $\nu i_{13/2}$ bands and negative-parity $\nu h_{9/2}$ bands of odd-A Yb isotopes are plotted in Fig. 6.

Some systematic features can be observed in Fig. 6. (1) The first band crossings in the positive-parity $\nu i_{13/2}$ bands of ^{161,163,165}Yb isotopes occur around almost same rotational frequencies, although these nuclei have different quadrupole deformations. This feature is also observed in the negative-parity $\nu h_{9/2}$ bands of ^{161,163,165}Yb isotopes. Taking into account the effect of blocking by the occupation of the quasineutron $\nu i_{13/2}$ configuration, the first band crossings in the $\nu i_{13/2}$ bands of ^{161,163,165}Yb have been ascribed to the alignment of $i_{13/2}(BC)$ neutron pair [1,3], while the $i_{13/2}(AB)$ neutron-pair alignment is responsible for the first band crossings in the $\nu h_{9/2}$ bands of ^{161,163,165}Yb [1,3]. The constant crossing frequency in ^{161,163,165}Yb isotopes has been explained in terms of the compensation between the decrease in the neutron-pair gap and the decrease in the alignment of the $i_{13/2}$ neutron pair with increasing neutron number [5]. (2) Both the first critical crossing frequencies of ^{157}Yb and ^{159}Yb have a little shifts compared to those of the heavier odd-A Yb isotopes. For the positive-parity $\nu i_{13/2}$ bands, the upbend observed in ^{159}Yb has been ascribed to the nearly simultaneous alignments of a pair of $h_{11/2}(ef)$ protons and a pair of $i_{13/2}(BC)$ neutrons [17], while the upbend observed in ^{157}Yb has been interpreted as simultaneous alignments of a pair of $h_{11/2}(ef)$ protons and a pair of $h_{9/2}(EF)$ neutrons [16]. The CSM calculations using the Woods-Saxon potential [41,42] for ^{157}Yb are presented in Fig. 7, where the deformation

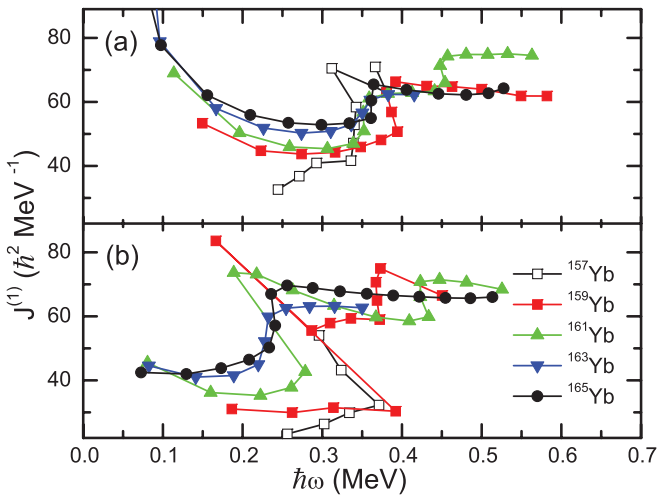

FIG. 6. (Color online) The kinematic moments of inertia as a function of rotational frequency for (a) the positive-parity $\nu i_{13/2}$ bands and (b) the negative-parity $\nu h_{9/2}$ bands in odd-A Yb isotopes.

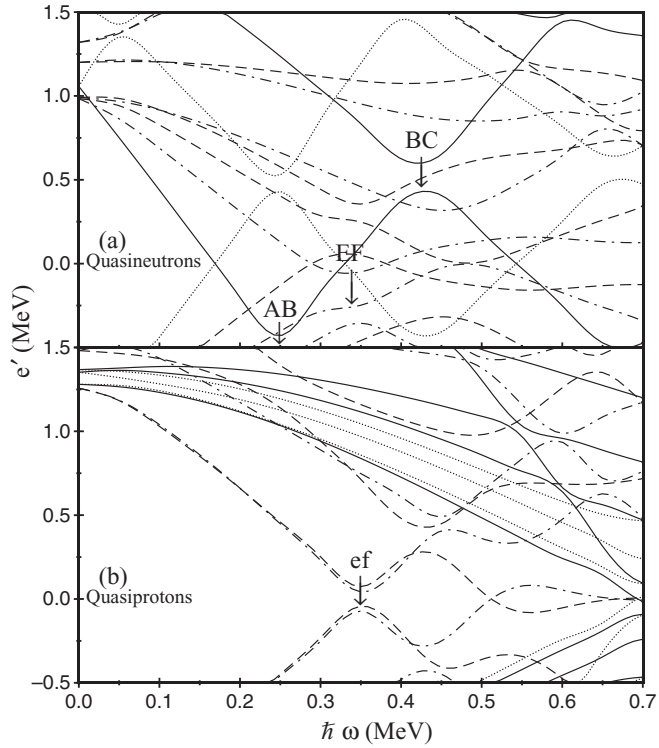

FIG. 7. Cranked Woods-Saxon Routhian diagrams for (a) quasineutrons and (b) quasiprotons in ^{157}Yb using deformation parameters, $\varepsilon_2 = 0.161$, $\varepsilon_4 = -0.037$, and $\gamma = 21^\circ$. Solid lines correspond to $(\pi, \alpha) = (+, +1/2)$, dotted lines $(+,-1/2)$, dot-dashed lines $(-,+1/2)$, and dashed lines $(-,-1/2)$.

parameters are derived from the TRS results. As shown in Fig. 7, the CSM calculations well reproduce the experimental values of ^{157}Yb for the critical frequencies and further confirm the cause of the upbend observed in ^{157}Yb. For the negative-parity $\nu h_{9/2}$ bands, the first backbends in ^{157}Yb and ^{159}Yb have been associated with the alignments of a pair of $h_{11/2}(ef)$ protons and a pair of $i_{13/2}(AB)$ neutrons, respectively [16,18].

The different patterns of band crossings between ^{157,159}Yb and heavier ^{161,163,165}Yb isotopes indicate that the inversion of the order of crossing frequency occurs as the neutron number decreases below $N = 91$. To straightforwardly illustrate the evolution of the crossing frequencies for specific quasiparticle in this mass region, the systematics of the $i_{13/2}(AB)$, $i_{13/2}(BC)$ neutron and $h_{11/2}(ef)$ proton crossing frequencies are plotted as a function of neutron number for Yb isotopes, as well as Er and Hf isotopes, in Fig. 8. The labeling convention for quasiparticles is given in Table V. As shown in Fig. 8(e), although the first band crossings in the negative-parity $\nu h_{9/2}$ bands of odd-A Yb and the even-A Yb isotopes are associated with the alignment of a same $\nu i_{13/2}(AB)$ neutron pair, the frequencies of the band crossings in the negative-parity $\nu h_{9/2}$ bands of odd-A Yb are a little lower than those in the yrast sequences of even-A Yb isotopes. This feature is also observed in the Er [Fig. 8(d)] and Hf [Fig. 8(f)] isotopes. Such a systematic shift can be attributed to the reduced neutron-pair correlations [3,5]. For the lighter Er, Yb, and Hf nuclei ($N < 90$), the frequencies of the $i_{13/2}$ paired neutron crossings

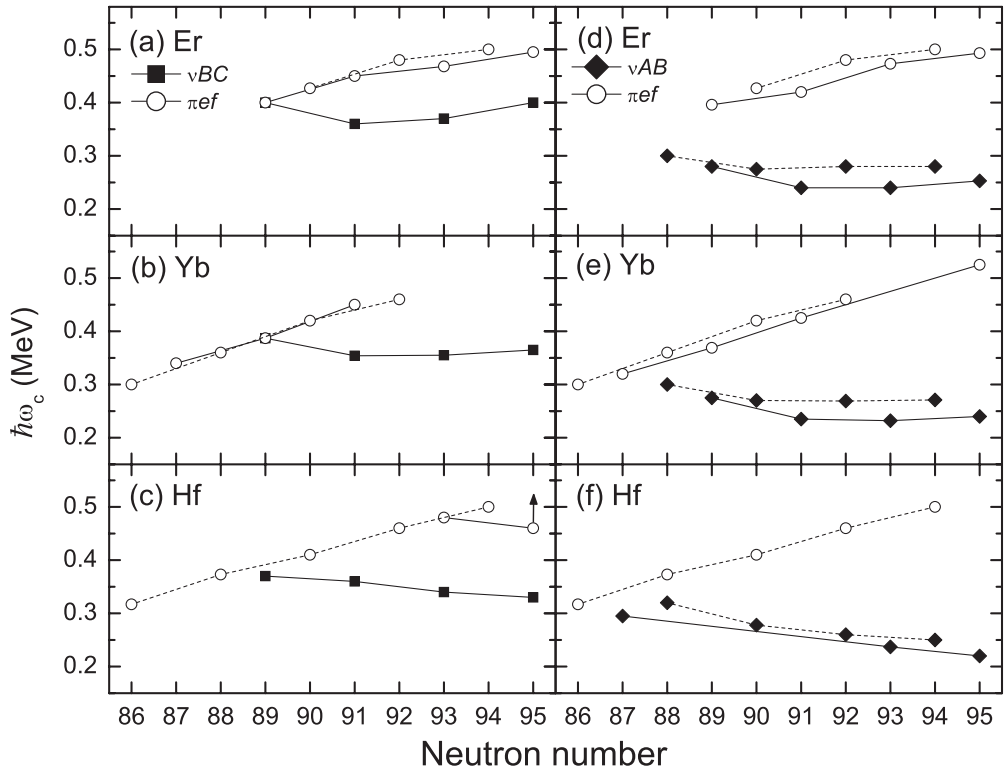

FIG. 8. Systematics of experimental crossing frequencies $\hbar\omega_c$ for the first $i_{13/2}(AB)$ neutron-pair (solid diamonds), second $i_{13/2}(BC)$ neutron-pair (solid squares), and the first $h_{11/2}(ef)$ proton-pair (open circles) alignments in the Er [4,30–32,43–50], Yb [1–3,7,15,16,18,36], and Hf [9,51–57] nuclei. The arrow indicates that only the lower limit can be deduced from the data. (a), (b), (c) The crossing frequencies of νBC and πef pair alignments are derived from the positive-parity $\nu i_{13/2}$ bands in odd-A nuclei; (d), (e), (f) the crossing frequencies of νAB and πef pair alignments are derived from the negative-parity $\nu h_{9/2}$ bands in odd-A nuclei. For the even-even nuclei, all the crossing frequencies are derived from the yrast bands except the ^{160}Hf nucleus, where only the $(\pi, \alpha) = (-, 1)$ band exhibits the $h_{11/2}(ef)$ proton-pair alignment.

are observed to increase with decreasing neutron number. Murzel *et al.* [9] have interpreted this behavior in terms of the position of the Fermi level. Because the Fermi level lies below the $i_{13/2}$ multiplet for these lighter nuclei, it needs more energy to excite a pair of quasiparticles into these states.

In contrast, the rotational frequency at which the $h_{11/2}(ef)$ proton pair aligns is observed to decrease with decreasing neutron number. The general trend of crossing frequency as a function of neutron number is consistent with the trend of the quadrupole deformation ε_2 for these nuclei. Therefore, the systematic behavior of crossing frequencies for the $h_{11/2}(ef)$ proton-pair alignment has been assumed to be predominantly attributable to the effect of quadrupole deformation, which is also supported by the CSM calculations [58]. For the positive-parity $\nu i_{13/2}$ bands of Yb isotopes, the different trends of the crossing frequencies for the $i_{13/2}(BC)$ neutron-pair alignment and the $h_{11/2}(ef)$ proton-pair alignment cause these two crossings to occur at the same place $N = 89$. This phenomenon is also observed in the Er isotopes. For the negative-parity $\nu h_{9/2}$ bands, owing to the lower crossing frequency of the $i_{13/2}(AB)$ neutron-pair alignment, the overlapping of these $i_{13/2}(AB)$ neutron-pair and $h_{11/2}(ef)$ proton-pair alignments occurs around $N \sim 87$.

It has been suggested that a pair of $i_{13/2}$ neutron alignment might be responsible for the observed first backbend in ^{158}Hf [51]. According to the systematic trend of crossing frequencies for the Hf isotopes shown in Fig. 8(f), the order of the $i_{13/2}(AB)$ neutron-pair and $h_{11/2}(ef)$ proton-pair alignments may already reverse at $N = 86$. Our TRS calculations also show that the alignment of an $h_{11/2}(ef)$ proton pair is responsible for the first backbend in ^{158}Hf. Thus, based on the empirical systematics and TRS calculations, we believe that the first band crossing observed in ^{158}Hf involves a pair of aligning $h_{11/2}$ protons. The $i_{13/2}$ neutron-pair alignment will occur at a little higher rotational frequency.

TABLE V. Convention for the quasiparticle labeling.

Label	Parity and signature (π, α)	Main shell model component
	Quasineutrons	
A	$(+, +1/2)_1$	$i_{13/2}$
B	$(+, -1/2)_1$	$i_{13/2}$
C	$(+, +1/2)_2$	$i_{13/2}$
E	$(-, +1/2)_1$	$h_{9/2}$
F	$(-, -1/2)_1$	$h_{9/2}$
	Quasiprotons	
e	$(-, +1/2)_1$	$h_{11/2}$
f	$(-, -1/2)_1$	$h_{11/2}$

VI. SUMMARY

The high-spin states in ^{157}Yb have been populated via ^{144}Sm(^{16}O,3n)^{157}Yb fusion-evaporation reaction and the resulting level scheme for ^{157}Yb is presented. The structures of rotational bands built on the intruder $i_{13/2}$ orbital and nonintruder $h_{9/2}$ orbital are studied within the framework of a triaxial PRM. Theoretical calculations further support the previous configuration assignments for these bands. Compared to the relative pure $i_{13/2}$ subshell components in the positive-parity band, there is a strong mixture of $h_{9/2}$ and $f_{7/2}$ subshells for the negative-parity band. As the nucleus rotates faster, the main component of both positive-parity and negative-parity bands are found to decrease gradually.

The isotopic dependence and frequency dependence of signature splitting in the positive-parity $\nu i_{13/2}$ bands of odd-A Yb isotopes are studied. According to the trend of the experimental signature splitting along with the neutron number and the theoretical calculations, the reason why the unfavored signature partner of the $\nu i_{13/2}$ band is not observed in ^{157}Yb can be ascribed to a very large signature splitting. For the signature splitting in the negative-parity $\nu h_{9/2}$ bands of odd-A Yb isotopes, the situation is a little more complicated. Owing to the enhanced interband $E1$ transitions in odd-A Yb isotopes, the low-spin parts of the unfavored signature partners of $\nu h_{9/2}$ bands are difficult to be experimentally observed. The characters of the signature splitting observed in ^{163}Yb can be qualitatively explained by the effect of changes in quadrupole and hexadecapole deformations. Based on the systematic comparison with the similar patterns observed in the heavier odd-A Yb isotopes, bands 1 and 2 in ^{157}Yb may form the signature partners of the $\nu h_{9/2}$ band.

With the new results of the ^{157}Yb nucleus and already known information on the neighboring nuclei, we make a systematic summary of the band crossing frequencies associated with the $i_{13/2}$ neutron-pair and $h_{11/2}$ proton-pair alignments for the Yb isotopes, as well as the Er and Hf isotopes. Their main features are discussed and the mechanisms behind the trends of the crossing frequencies are analyzed. Based on the systematics and TRS calculations, we reinterpret the cause of first band crossing observed in ^{158}Hf nucleus.

ACKNOWLEDGMENTS

This work is support by the Natural Science Foundation of China under Grants No. 11175003, No. 11235001, No. 10975007, No. 11175108, and No. J1103206 and the Chinese Major State Basic Research Development Program Grant No. 2013CB834400. The authors wish to thank G. J. Xu and Q. W. Fan for making the target and the staff in the tandem accelerator laboratory at the CIAE, Beijing.

[1] L. L. Riedinger, Nucl. Phys. A **347**, 141 (1980).
[2] N. Roy, S. Jónsson, H. Ryde, W. Waluś, J. J. Gaardhøje, J. D. Garrett, G. B. Hagemann, and B. Herskind, Nucl. Phys. A **382**, 125 (1982).
[3] J. Kownacki, J. D. Garrett, J. J. Gaardhøje, G. B. Hagemann, B. Herskind, S. Jónsson, N. Roy, H. Ryde, and W. Waluś, Nucl. Phys. A **394**, 269 (1983).
[4] M. A. Riley, J. Simpson, R. Aryaeinejad, J. R. Cresswell, P. D. Forsyth, D. Howe, P. J. Nolan, B. M. Nyakó, J. F. Sharpey-Schafer, P. J. Twin, J. Bacelar, J. D. Garrett, G. B. Hagemann, B. Herskind, and A. Holm, Phys. Lett. B **135**, 275 (1984).
[5] S. Jónsson, N. Roy, H. Ryde, W. Waluś, J. Kownacki, J. D. Garrett, G. B. Hagemann, B. Herskind, R. Bengtsson, and S. Åberg, Nucl. Phys. A **449**, 537 (1986).
[6] S. Shastry, J. C. Bacelar, J. D. Garrett, G. B. Hagemann, B. Herskind, and J. Kownacki, Nucl. Phys. A **470**, 253 (1987).
[7] J. N. Mo, S. Sergiwa, R. Chapman, J. C. Lisle, E. Paul, J. C. Willmott, J. Hattula, M. Jääskeläinen, J. Simpson, P. M. Walker, J. D. Garrett, G. B. Hagemann, B. Herskind, M. A. Riley, and G. Sletten, Nucl. Phys. A **472**, 295 (1987).
[8] J. Simpson, M. A. Riley, J. F. Sharpey-Schafer, J. C. Bacelar, A. P. Cook, J. R. Cresswell, D. V. Elenkov, P. D. Forsyth, G. B. Hagemann, B. Herskind, A. Holm, D. Howe, and B. M. Nyakó, J. Phys. G **15**, 643 (1989).
[9] M. Murzel, U. Birkental, K. P. Blume, S. Heppner, H. Hübel, J. Recht, W. Schmitz, K. Theine, H. Kluge, A. Kuhnert, K. H. Maier, G. Hebbinghaus, and H. Schnare, Nucl. Phys. A **516**, 189 (1990).
[10] J. Simpson, M. A. Riley, A. Alderson, M. A. Bentley, A. M. Bruce, D. M. Cullen, P. Fallon, F. Hanna, and L. Walker, J. Phys. G **17**, 511 (1991).
[11] W. F. Mueller, H. J. Jensen, W. Reviol, L. L. Riedinger, C.-H. Yu, J.-Y. Zhang, W. Nazarewicz, and R. Wyss, Phys. Rev. C **50**, 1901 (1994).
[12] D. J. Hartley, M. A. Riley, D. E. Archer, T. B. Brown, J. Döring, R. A. Kaye, F. G. Kondev, T. Petters, J. Pfohl, R. K. Sheline, S. L. Tabor, and J. Simpson, Phys. Rev. C **57**, 2944 (1998).
[13] D. G. Roux, M. S. Fetea, E. Gueorguieva, B. R. S. Babu, R. T. Newman, J. J. Lawrie, R. Fearick, D. G. Aschman, R. Beetge, M. Benatar, G. K. Mabala, S. M. Mullins, S. H. T. Murray, S. Naguleswaran, C. Rigollet, J. F. Sharpey-Schafer, F. D. Smit, and W. J. Whittaker, Phys. Rev. C **63**, 024303 (2001).
[14] A. Pipidis *et al.*, Phys. Rev. C **72**, 064307 (2005).
[15] Z. Y. Li *et al.*, Phys. Rev. C **77**, 064323 (2008).
[16] C. Xu *et al.*, Phys. Rev. C **83**, 014318 (2011).
[17] T. Byrski, F. A. Beck, J. C. Merdinger, A. Nourreddine, H. W. Cranmer-Gordon, D. V. Elenkov, P. D. Forsyth, D. Howe, M. A. Riley, J. F. Sharpey-Schafer, J. Simpson, J. Dudek, and W. Nazarewicz, Nucl. Phys. A **474**, 193 (1987).
[18] D. B. Campbell, Ph.D. thesis, Florida State University, 2004.
[19] C. Schuck, N. Bendjaballah, R. M. Diamond, Y. Ellis-Akovali, K. H. Lindenberger, J. O. Newton, F. S. Stephens, J. D. Garrett, and B. Herskind, Phys. Lett. B **142**, 253 (1984).
[20] M. H. Rafailovich, O. C. Kistner, A. W. Sunyar, S. Vajda, and G. D. Sprouse, Phys. Rev. C **30**, 169 (1984).
[21] B. Qi, S. Q. Zhang, S. Y. Wang, and J. Meng, Int. J. Mod. Phys. E **18**, 109 (2009).
[22] S. E. Larsson, G. Leander, and I. Ragnarsson, Nucl. Phys. A **307**, 189 (1978).
[23] I. Ragnarsson and P. B. Semmes, Hyperfine Interact. **43**, 425 (1988).

[24] S. Q. Zhang, B. Qi, S. Y. Wang, and J. Meng, Phys. Rev. C **75**, 044307 (2007).
[25] T. Bengtsson and I. Ragnarsson, Nucl. Phys. A **436**, 14 (1985).
[26] W. Satuła, R. Wyss, and P. Magierski, Nucl. Phys. A **578**, 45 (1994).
[27] F. R. Xu, W. Satuła, and R. Wyss, Nucl. Phys. A **669**, 119 (2000).
[28] C. S. Wu and J. Y. Zeng, Commun. Theor. Phys. **8**, 51 (1987).
[29] S. G. Nilsson, C. F. Tsang, A. Sobiczewski, Z. Szymański, S. Wycech, C. Gustafson, I.-L. Lamm, P. Möller, and B. Nilsson, Nucl. Phys. A **131**, 1 (1969).
[30] Evaluated Nuclear Structure Data File (ENSDF), http://www.nndc.bnl.gov/ensdf
[31] L. Chen *et al.*, Phys. Rev. C **83**, 034318 (2011).
[32] G. B. Hagemann, H. Ryde, P. Bosetti, A. Brockstedt, H. Carlsson, L. P. Ekström, A. Nordlund, R. A. Bark, B. Herskind, S. Leoni, A. Bracco, F. Camera, S. Frattini, M. Mattiuzzi, B. Million, C. Rossi-Alvarez, G. de Angelis, D. Bazzacco, S. Lunardi, and M. De Poli, Nucl. Phys. A **618**, 199 (1997).
[33] S. T. Wang, X. H. Zhou, Y. H. Zhang, Y. Zheng, M. L. Liu, F. Ma, J. Hu, L. Chen, X. Zhang, N. T. Zhang, L. H. Zhu, X. G. Wu, and G. S. Li, Chin. Phys. C **33**, 629 (2009).
[34] I. Hamamoto, J. Höller, and X. Z. Zhang, Phys. Lett. B **226**, 17 (1989).
[35] G. B. Hagemann, I. Hamamoto, and W. Satuła, Phys. Rev. C **47**, 2008 (1993).
[36] S. B. Patel, F. S. Stephens, J. C. Bacelar, E. M. Beck, M. A. Deleplanque, R. M. Diamond, and J. E. Draper, Phys. Rev. Lett. **57**, 62 (1986).
[37] R. A. Bark, J. F. Sharpey-Schafer, S. M. Maliage, T. E. Madiba, F. S. Komati, E. A. Lawrie, J. J. Lawrie, R. Lindsay, P. Maine, S. M. Mullins, S. H. T. Murray, N. J. Ncapayi, T. M. Ramashidza, F. D. Smit, and P. Vymers, Phys. Rev. Lett. **104**, 022501 (2010).
[38] F. K. McGowan, N. R. Johnson, C. Baktash, I. Y. Lee, Y. Schutz, J. C. Wells, and A. Larabee, Nucl. Phys. A **539**, 276 (1992).
[39] J. D. Garrett, in *Proceedings of the XX International Winter Meeting on Nuclear Physics, Bormio, Italy, 1982*, edited by I. Iori (Ricerca Scientifica ed Educazione Permanente, Milano, 1982), p. 1.
[40] J. Nyberg, A. Johnson, M. P. Carpenter, C. R. Bingham, L. H. Courtney, V. P. Janzen, S. Juutinen, A. J. Larabee, Z.-M. Liu, L. L. Riedinger, C. Baktash, M. L. Halbert, N. R. Johnson, I. Y. Lee, Y. Schutz, J. C. Waddington, and D. G. Popescu, Nucl. Phys. A **511**, 92 (1990).
[41] W. Nazarewicz, J. Dudek, R. Bengtsson, and I. Ragnarsson, Nucl. Phys. A **435**, 397 (1985).
[42] S. Ćwiok, J. Dudek, W. Nazarewicz, K. Skalski, and T. Werner, Comput. Phys. Commun. **46**, 379 (1987).
[43] J. Simpson, M. A. Riley, J. R. Cresswell, D. V. Elenkov, P. D. Forsyth, G. B. Hagemann, D. Howe, B. M. Nyakó, S. Ogaza, J. C. Lisle, and J. F. Sharpey-Schafer, J. Phys. G **13**, 847 (1987).
[44] J. Simpson, P. A. Butler, P. D. Forsyth, J. F. Sharpey-Schafer, J. D. Garrett, G. B. Hagemann, B. Herskind, and L. P. Ekström, J. Phys. G **10**, 383 (1984).
[45] E. S. Paul, S. V. Rigby, M. A. Riley, J. Simpson, D. E. Appelbe, D. B. Campbell, P. T. W. Choy, R. M. Clark, M. Cromaz, A. O. Evans, P. Fallon, A. Görgen, D. T. Joss, I. Y. Lee, A. O. Macchiavelli, P. J. Nolan, A. Pipidis, D. Ward, and I. Ragnarsson, Phys. Rev. C **79**, 044324 (2009).
[46] A. O. Evans, E. S. Paul, J. Simpson, M. A. Riley, D. E. Appelbe, D. B. Campbell, P. T. W. Choy, R. M. Clark, M. Cromaz, P. Fallon, A. Görgen, D. T. Joss, I. Y. Lee, A. O. Macchiavelli, P. J. Nolan, A. Pipidis, D. Ward, and I. Ragnarsson, Phys. Rev. C **73**, 064303 (2006).
[47] M. Mustafa *et al.*, Phys. Rev. C **84**, 054320 (2011).
[48] J. Ollier *et al.*, Phys. Rev. C **83**, 044309 (2011).
[49] M. A. Riley, J. W. Roberts, J. Simpson, A. Alderson, I. Ali, M. A. Bentley, A. M. Bruce, R. Chapman, D. M. Cullen, P. Fallon, P. D. Forsyth, J. C. Lisle, J. N. Mo, and J. F. Sharpey-Schafer, J. Phys. G **16**, L67 (1990).
[50] J. Simpson, A. P. Bagshaw, A. Pipidis, M. A. Riley, M. A. Bentley, D. M. Cullen, P. J. Dagnall, G. B. Hagemann, S. L. King, R. W. Laird, J. C. Lisle, S. Shepherd, A. G. Smith, S. Törmänen, A. V. Afanasjev, and I. Ragnarsson, Phys. Rev. C **62**, 024321 (2000).
[51] K. Y. Ding, J. A. Cizewski, D. Seweryniak, H. Amro, M. P. Carpenter, C. N. Davids, N. Fotiades, R. V. F. Janssens, T. Lauritsen, C. J. Lister, D. Nisius, P. Reiter, J. Uusitalo, I. Wiedenhöver, and A. O. Macchiavelli, Phys. Rev. C **62**, 034316 (2000).
[52] H. Hübel, M. Murzel, E. M. Beck, H. Kluge, A. Kuhnert, K. H. Maier, J. C. Bacelar, M. A. Deleplanque, R. M. Diamond, and F. S. Stephens, Z. Phys. A **329**, 289 (1988).
[53] K. P. Blume, H. Hübel, M. Murzel, J. Recht, K. Theine, H. Kluge, A. Kuhnert, K. H. Maier, A. Maj, M. Guttormsen, and A. P. De Lima, Nucl. Phys. A **464**, 445 (1987).
[54] M. Neffgen, E. M. Beck, H. Hübel, J. C. Bacelar, M. A. Deleplanque, R. M. Diamond, F. S. Stephens, and J. E. Draper, Z. Phys. A **344**, 235 (1993).
[55] D. R. Jensen *et al.*, Eur. Phys. J. A **8**, 165 (2000).
[56] M. Cromaz, J. DeGraaf, T. E. Drake, D. Ward, A. Galindo-Uribarri, V. P. Janzen, D. C. Radford, S. Flibotte, S. M. Mullins, J. Rodriguez, and S. Pilotte, Phys. Rev. C **59**, 2406 (1999).
[57] M. B. Smith, G. J. Campbell, R. Chapman, P. O. Tjøm, R. A. Bark, G. B. Hagemann, N. Keeley, D. J. Middleton, H. Ryde, and K.-M. Spohr, Eur. Phys. J. A **6**, 37 (1999).
[58] R. Bengtsson and S. Frauendorf, Nucl. Phys. A **327**, 139 (1979).